The Astrophysical Journal Letters, 892:L16 (6pp), 2020 March 20 https://doi.org/10.3847/2041-8213/ab7cd8


# Thunder and Lightning: Using Neutron-star Mergers as Simultaneous Standard Candles and Sirens to Measure Cosmological Parameters

Zoheyr Doctor
Department of Physics, University of Oregon, Eugene, OR 97403, USA; zoheyr.doctor@gmail.com
*Received 2019 December 27; revised 2020 March 3; accepted 2020 March 4; published 2020 March 25*

## Abstract

With the detection of gravitational wave (GW) GW170817 and its associated electromagnetic (EM) counterparts from a binary neutron star (NS) merger, the "standard siren" method for Hubble-constant measurements is expected to play a role in the Hubble-constant tension in the next few years. One intriguing proposal put forward in multiple studies is to use an NS merger's optical counterpart, known as a kilonova, as a standard candle, because its absolute magnitude can in principle be calculated from simulations. In this work, I detail the statistical framework for performing joint standard-candle and standard-siren measurements using GWs, EM follow-up data, and simulations of EM counterparts. I then perform an example analysis using GW170817 and its optical counterpart AT2017gfo to illustrate the method and the method's limitations. Crucially, the inferences using this method are only as robust as the EM counterpart models, so significant theoretical advances are needed before this method can be employed for precision cosmology.

*Unified Astronomy Thesaurus concepts:* Neutron stars (1108); Hubble constant (758); Cosmological parameters (339); Gravitational waves (678)

## 1. Introduction

With tensions mounting in the cosmology community over the value of the Hubble constant (Riess et al. 2016; Freedman 2017; Planck Collaboration 2018), new and independent measurements of cosmological parameters have gained significant interest. The most provocative of these new measurements employs gravitational waves (GWs) from compact-object mergers and their associated electromagnetic (EM) counterparts as "standard sirens" to estimate $H_0$, the Hubble constant (Schutz 1986; Holz & Hughes 2005; Del Pozzo 2014; Abbott et al. 2017b; Chen et al. 2018; Mortlock et al. 2019; Soares-Santos et al. 2019). These standard-siren measurements differ from traditional distance-ladder measurements in that the luminosity distance to the source can be directly inferred from the GW signal without the need of empirical calibration of increasingly distant sources. For GW170817, the first GW detected from a neutron-star (NS) merger and the first to have associated EM counterparts, Abbott et al. (2017b) inferred $H_0 = 70.0^{+12.0}_{-8.0}$ (maximum a posteriori with 68% credible interval), which, while exciting, was alone not enough to significantly tip the scales on the Hubble-constant controversy. The second reported GW of potential NS binary origin, GW190425 (Abbott et al. 2020), did not have an identified host galaxy (e.g., Coughlin et al. 2019a; Hosseinzadeh et al. 2019), and therefore offered no additional $H_0$ constraints. Nevertheless, combining the GW170817 estimate with future standard-siren analyses is expected to yield a competitive $H_0$ measurement with $O(100)$ GWs with identified host galaxies (Chen et al. 2018). Furthermore, EM counterpart morphology can be leveraged to infer the inclination angle of the binary inspiral and break the well-known distance-inclination degeneracy, leading to improved estimates of $H_0$ (Abbott et al. 2017b; Guidorzi et al. 2017; Dhawan et al. 2020).

Until recently, no one had considered leveraging the optical data from an NS merger to directly infer the source luminosity distance, enabling a standard-candle measurement using an EM counterpart. New studies in Kashyap et al. (2019) and Coughlin et al. (2019c) have explored this possibility and treated the prompt, thermal radiation from neutron-rich ejecta from the merger, known as a kilonova (KN), as a standard candle. Using simulations of NS merger ejecta, Kashyap et al. (2019) find a clear relationship between the slope and the peak brightness of the KN bolometric light curves under certain assumptions, suggesting that KNe could be "standardized." Coughlin et al. (2019c) found similar correlations between light curve stretch and brightness in KN simulations and use fits to these correlations to infer $H_0$ with GW170817 as a standard candle. Also, they combine the $H_0$ posteriors of the GW170817 standard-candle and standard-siren analyses to produce a joint $H_0$ fit. While these analyses have crucially laid the groundwork for joint GW–EM inference of $H_0$, neither has presented the full Bayesian approach for performing these inferences with an arbitrary EM counterpart.

In this Letter, I present a method for performing joint GW–EM $H_0$ inferences and enumerate some of the technical subtleties that can affect the measurements. In this method, the luminosity distance to the source is simultaneously fit using the GW with the light curves and/or spectra of the EM counterparts, drawing an analogy with estimating the distance to a lighting strike using both the brightness of the lightning and the loudness of the thunder. (Though unlike lightning and thunder, light and GWs travel at the same speed). This basically amounts to including the EM counterpart *likelihood* in the standard-siren calculation.[1] By including this likelihood, the luminosity distance to the source (and hence the cosmological parameter inference) is further constrained by the observed EM counterpart morphology.

The layout of this Letter is as follows: in Section 2, I present the Bayesian framework for performing "thunder-and-lightning" inferences of $H_0$. In Section 3 I perform an example thunder-and-lightning $H_0$ measurement with GW170817 and its bolometric light curve. One essential takeaway from

[1] Note that the calculation is *not* a simple multiplication of EM- and GW-based distance posteriors as claimed in Coughlin et al. (2019c).

Section 3 is that systematic errors in the underlying EM counterpart models can significantly affect the cosmological inferences. It is not clear that currently available models are sufficiently systematics-free to be employed for precision cosmology, so I do not attempt to stack multiple simulated events in this work, but future work could explore this. Finally, in Sections 4 and 5, I conclude by offering some high-level discussion on the method presented herein and future prospects.

## 2. Statistical Framework

I develop a Bayesian framework for making thunder-and-lightning inferences of the Hubble constant (and other cosmological parameters), which incorporates both GW- and EM-follow-up data. The framework makes use of the following ingredients.

1. Data:
   (a) GW data $x_{\rm GW}$: the strain time series in $N$ different detectors $\{h_i(t)\}_{i=1}^{N}$.
   (b) EM counterpart data $x_{\rm EM}$: counts or flux measurements of the EM counterpart. This could be in multiple bands and/or with multiple instruments.
   (c) Host-galaxy recessional velocity $v_r$: measured through spectroscopy of the host galaxy.
   (d) Peculiar velocity field $\langle v_p \rangle$ of the host galaxy group: a measurement of the peculiar velocity field in the vicinity of the host galaxy. In Abbott et al. (2017b), this was computed through a weighted average of the peculiar radial velocities of galaxies nearby the host.
2. Models/Assumptions:
   (a) Gravitational waveform model: a model for the GW strain as a function of intrinsic source parameters (masses, spins, and equation of state of the compact binary) and extrinsic parameters (e.g., luminosity distance, sky position, inclination). Contemporary examples include the models of Dietrich et al. (2019) and Lackey et al. (2019).
   (b) EM counterpart model: a forward model for $x_{\rm EM}$ that is a function of the compact binary parameters. This could be a hierarchical model that predicts some EM counterpart parameters (e.g., ejected mass or jet opening angle) based on the binary parameters, and then predicts $x_{\rm EM}$ via the EM counterpart parameters. For example, Coughlin et al. (2019d, 2018) and Abbott et al. (2017c) provide state-of-the-art forward models of KNe.
   (c) Recessional velocity model: a model for the observed recessional velocity of the host given its peculiar velocity and a cosmology. See Abbott et al. (2017b) for an example.
   (d) Peculiar velocity field model: a model for the measured peculiar velocity field in the vicinity of the host galaxy given the host galaxy peculiar radial velocity. See Abbott et al. (2017b) for an example.

With these pieces in hand, one can compute the likelihood of the data set given the cosmological parameters $\boldsymbol{\theta}_c$ and the models. Following Abbott et al. (2017b) I can write the likelihood as

$$\mathcal{L}(x_{\rm GW}, x_{\rm EM}, v_r, \langle v_p \rangle | \boldsymbol{\theta}_c) = \frac{p(x_{\rm GW}, x_{\rm EM}, v_r, \langle v_p \rangle | \boldsymbol{\theta}_c)}{\int_{\rm det} p(x_{\rm GW}, x_{\rm EM}, v_r, \langle v_p \rangle | \boldsymbol{\theta}_c) dx_{\rm GW} dx_{\rm EM} dv_r d\langle v_p \rangle}. \quad (1)$$

The denominator term depends only on $\boldsymbol{\theta}_c$ and appropriately renormalizes the likelihood to be the likelihood over *detectable* events (Abbott et al. 2017b; Chen et al. 2018). The integral is taken over data sets that meet some detection threshold and represents the fraction of all possible data sets, conditioned on $\boldsymbol{\theta}_c$, which would be included in this analysis.

To see the dependence of the data on the cosmological parameters, I expand the numerator term as follows:

$$\begin{aligned} & p(x_{\rm GW}, x_{\rm EM}, v_r, \langle v_p \rangle | \boldsymbol{\theta}_c) \\ &= \int p(x_{\rm GW}, x_{\rm EM}, v_r, \langle v_p \rangle, \boldsymbol{\theta}, d_L, z, i, v_p | \boldsymbol{\theta}_c) d\boldsymbol{\theta} dd_L dz di dv_p \\ &= \int p(x_{\rm GW}, x_{\rm EM}, v_r, \langle v_p \rangle | \boldsymbol{\theta}_c, \boldsymbol{\theta}, d_L, z, i, v_p) \\ &\quad \times p(\theta, d_L, z, i | \boldsymbol{\theta}_c) p(v_p) d\boldsymbol{\theta} dd_L dz di dv_p \\ &= \int p(x_{\rm GW} | \boldsymbol{\theta}_c, \boldsymbol{\theta}, d_L, z, i) \\ &\quad \times p(x_{\rm EM} | \boldsymbol{\theta}_c, \boldsymbol{\theta}, d_L, z, i) p(v_r, \langle v_p \rangle | \boldsymbol{\theta}_c, \boldsymbol{\theta}, d_L, z, i, v_p) \\ &\quad \times p(\boldsymbol{\theta}, d_L, z, i | \boldsymbol{\theta}_c) p(v_p) d\boldsymbol{\theta} dd_L dz di dv_p \\ &= \int p(x_{\rm GW} | \boldsymbol{\theta}, d_L, z, i) p(x_{\rm EM} | \boldsymbol{\theta}, d_L, z, i) p(v_r, \langle v_p \rangle | z, v_p) \\ &\quad \times p(\boldsymbol{\theta}) p(z | d_L, \boldsymbol{\theta}_c) p(d_L) p(i) p(v_p) d\boldsymbol{\theta} dd_L dz di dv_p \end{aligned} \quad (2)$$

$d_L$, $z$, and $i$, and $v_p$ are the source's luminosity distance, redshift, inclination angle, and host-galaxy peculiar velocity, respectively, and $\boldsymbol{\theta}$ is the array of remaining parameters that describe the binary system, such as total mass, mass ratio, spins, and equation of state. Going from the first to second line of Equation (2), I apply Bayes' Rule. In the third line, I split individual likelihoods under the assumption that the GW data, EM data, and measured velocities are independent. Then in the final line I separate the priors on $\boldsymbol{\theta}_c$, $d_L$, and $i$ by assuming they are independent and remove the explicit $\boldsymbol{\theta}_c$ dependence of $x_{\rm EM}$, $x_{\rm GW}$, $v_r$, and $\langle v_p \rangle$ because those are fully specified by $d_L$ and $z$. Note that I assume that $v_p$ negligibly affects the measured GW or EM counterpart data. $z$ is fully specified by $d_L$ and cosmology, so $p(z|d_L, \boldsymbol{\theta}_c) = \delta(\tilde{z} - z)$ where $\tilde{z} = z(d_L, \boldsymbol{\theta}_c)$. This leaves

$$\begin{aligned} p(x_{\rm GW}, x_{\rm EM}, v_r, \langle v_p \rangle | \boldsymbol{\theta}_c) = \int & p(x_{\rm GW} | \boldsymbol{\theta}, d_L, \tilde{z}, i) \\ & \times p(x_{\rm EM} | \boldsymbol{\theta}, d_L, \tilde{z}, i) p(v_r, \langle v_p \rangle | \tilde{z}, v_p) \\ & \times p(\boldsymbol{\theta}) p(d_L) p(i) p(v_p) d\boldsymbol{\theta} dd_L di dv_p. \end{aligned} \quad (3)$$

Now I turn to the second term in the integrand, which is the likelihood of the EM follow-up data. In general, it is not straightforward to predict the EM data directly from the binary parameters, but a number of studies have attempted to do this via EM counterpart ansatz parameters $\boldsymbol{\theta}_{\rm EM}$. For example, a number of models parameterize KN spectra in terms of the mass, velocity, and composition of the material ejected in the NS merger (e.g., Kasen et al. 2017; Coughlin et al. 2018; Bulla 2019; Metzger 2019). These parameters can in turn be predicted from the binary system parameters with the help of

NS merger simulations. We can therefore expand the EM likelihood as

$$p(x_{\rm EM}|\boldsymbol{\theta}, \tilde{d}_L, \tilde{z}, i) = \int p(x_{\rm EM}, \boldsymbol{\theta}_{\rm EM}|\boldsymbol{\theta}, \tilde{d}_L, \tilde{z}, i) d\boldsymbol{\theta}_{\rm EM} = \int p(x_{\rm EM}|\boldsymbol{\theta}_{\rm EM}, \tilde{d}_L, \tilde{z}, i) p(\boldsymbol{\theta}_{\rm EM}|\boldsymbol{\theta}) d\boldsymbol{\theta}_{\rm EM} \quad (4)$$

The term $p(\boldsymbol{\theta}_{\rm EM}|\boldsymbol{\theta})$ enables us to encode our uncertainty about the EM counterpart parameters based on the binary parameters, which may be helpful in cases where there is significant error or uncertainty in the ansatz simulations. However, in principle, $\boldsymbol{\theta}_{\rm EM}$ should be fully predicted by $\boldsymbol{\theta}$, in which case $p(x_{\rm EM}|\boldsymbol{\theta}, \tilde{d}_L, \tilde{z}, i) = p(x_{\rm EM}|\boldsymbol{\theta}_{\rm EM}(\boldsymbol{\theta}), \tilde{d}_L, \tilde{z}, i)$. Wrapping this all together into a final posterior distribution on the cosmological parameters yields

$$p(\boldsymbol{\theta}_c|x_{\rm GW}, x_{\rm EM}, v_r, \langle v_p \rangle) = \frac{p(\boldsymbol{\theta}_c)}{\beta(\boldsymbol{\theta}_c)} \int p(x_{\rm GW}|\boldsymbol{\theta}, d_L, \tilde{z}, i) \times p(x_{\rm EM}|\boldsymbol{\theta}_{\rm EM}, d_L, \tilde{z}, i) p(\boldsymbol{\theta}_{\rm EM}|\boldsymbol{\theta}) \times p(v_r, \langle v_p \rangle | \tilde{z}, v_p) p(\boldsymbol{\theta}) p(d_L) p(i) p(v_p) \times d\boldsymbol{\theta}_{\rm EM} d\boldsymbol{\theta} dd_L di dv_p \quad (5)$$

where

$$\beta(\boldsymbol{\theta}_c) = \int\int_{\substack{x_{\rm GW}, x_{\rm EM}, \\ v_r, \langle v_p \rangle \in \det}} p(x_{\rm GW}, x_{\rm EM}, v_r, \langle v_p \rangle | \times \boldsymbol{\theta}, \boldsymbol{\theta}_{\rm EM}, d_L, \tilde{z}, i, v_p) p(\boldsymbol{\theta}_{\rm EM}|\boldsymbol{\theta}) \times p(\boldsymbol{\theta}) p(d_L) p(i) p(v_p) dx_{\rm GW} dx_{\rm EM} dv_r d\langle v_p \rangle \times d\boldsymbol{\theta}_{\rm EM} d\boldsymbol{\theta} dd_L di dv_p. \quad (6)$$

### 2.1. Selection Effects

The denominator term in the likelihood $\beta(\boldsymbol{\theta}_c)$ that accounts for selection effects has been discussed in other work on these types of measurements (Abbott et al. 2017b; Chen et al. 2018), and it can vary in computational complexity depending on the situation and assumptions made. In cases where the EM and GW detection probabilities are unaffected by cosmology (e.g., at low redshift), the denominator term can be ignored, as was done in Abbott et al. (2017b). In the general case though, it must be computed, because the cosmological parameters affect the GW signal frequency band (detector frame), the sky-map area, and the EM counterpart brightness in the search filters, and hence affect the probability of detection.

Before expanding $\beta(\boldsymbol{\theta}_c)$, I first make some simplifying assumptions. I assume that detection of $x_{\rm EM}$ enforces detection of $v_r$ and $\langle v_p \rangle$ and hence combine the recessional velocity data into the variable $x_{\rm EM}$. This is a reasonable assumption because if an EM counterpart is pinpointed, its host galaxy redshift can be readily measured spectroscopically. A second stipulation that I make is that the detection of EM data is conditioned on detection of GW data. While it is possible to do sub-threshold searches for GW events based on serendipitous detection of KNe (Doctor et al. 2017; Scolnic et al. 2018), gamma-ray bursts (Harstad 2013; Abbott et al. 2017a), or other counterparts, the vast majority of joint GW–EM detections will come from a GW detection triggering an EM search. With these assumptions, $\beta(\boldsymbol{\theta}_c)$ is

$$\begin{aligned}\beta(\boldsymbol{\theta}_c) &= \int\int_{\substack{x_{\rm GW}, x_{\rm EM} \\ \in \det}} p(x_{\rm GW}, x_{\rm EM}|\boldsymbol{\theta}, \boldsymbol{\theta}_{\rm EM}, d_L, \tilde{z}, i) \times p(\boldsymbol{\theta}_{\rm EM}|\boldsymbol{\theta}) p(\boldsymbol{\theta}) p(d_L) p(i) p(v_p) \times dx_{\rm GW} dx_{\rm EM} d\boldsymbol{\theta}_{\rm EM} d\boldsymbol{\theta} dd_L di \\ &= \int\int_{\substack{x_{\rm GW} \\ \in \det}} p_{\rm det}^{\rm EM}(x_{\rm GW}, \boldsymbol{\theta}_{\rm EM}, d_L, \tilde{z}, i) p(x_{\rm GW}|\boldsymbol{\theta}, d_L, \tilde{z}, i) \times p(\boldsymbol{\theta}_{\rm EM}|\boldsymbol{\theta}) p(\boldsymbol{\theta}) p(d_L) p(i) p(v_p) \times dx_{\rm GW} d\boldsymbol{\theta}_{\rm EM} d\boldsymbol{\theta} dd_L di \\ &= \int p_{\rm det}^{\rm EM,GW}(\boldsymbol{\theta}_{\rm EM}, \boldsymbol{\theta}, d_L, \tilde{z}, i) p(\boldsymbol{\theta}_{\rm EM}|\boldsymbol{\theta}) \times p(\boldsymbol{\theta}) p(d_L) p(i) p(v_p) dx_{\rm GW} d\boldsymbol{\theta}_{\rm EM} d\boldsymbol{\theta} dd_L di \end{aligned} \quad (7)$$

where

$$p_{\rm det}^{\rm EM}(x_{\rm GW}, \boldsymbol{\theta}_{\rm EM}, d_L, \tilde{z}, i) = \int_{x_{\rm EM} \in \det} p(x_{\rm EM}|x_{\rm GW}, \boldsymbol{\theta}_{\rm EM}, d_L, \tilde{z}, i) dx_{\rm EM} \quad (8)$$

$$p_{\rm det}^{\rm EM,GW}(\boldsymbol{\theta}_{\rm EM}, \boldsymbol{\theta}, d_L, \tilde{z}, i) = \int_{x_{\rm GW} \in \det} p_{\rm det}^{\rm EM}(x_{\rm GW}, \boldsymbol{\theta}_{\rm EM}, d_L, \tilde{z}, i) p(x_{\rm GW}|\boldsymbol{\theta}, d_L, \tilde{z}, i) dx_{\rm GW}. \quad (9)$$

Equations (8) and (9) are the probability of detection of the EM counterpart given the GW data, source properties, and cosmology, and the probability of detection of both the EM counterpart *and* the GW given the source properties and cosmology, respectively.

I will not attempt to calculate $\beta(\boldsymbol{\theta}_c)$ for arbitrary experimental configurations here, and instead I will simply comment on what considerations must go into computing it, if it is needed. As noted in Abbott et al. (2017b), $\beta(\boldsymbol{\theta}_c)$ can be ignored in cases where the GW selection effects dominate and the GW binary NS detection horizon distance is small. The selection effect on GWs is largely driven by the GW signal-to-noise ratio $\rho$, which will not change appreciably for the slight redshifting of the GW signal expected at such small distances (below a few hundred Mpc). Therefore, there is no selection of the data set that is conditioned on the cosmological parameters, and one can safely ignore $\beta$. However, for larger GW horizon distances, substantial redshifting of the GW signals (that depends on $\boldsymbol{\theta}_c$) can change detection prospects, and $\beta(\boldsymbol{\theta}_c)$ must be explicitly calculated.

If we now consider sources that are detectable at cosmological distances, we must estimate $\beta(\boldsymbol{\theta}_c)$. While $\beta(\boldsymbol{\theta}_c)$ could be directly computed by, e.g., Monte Carlo integration if the full model and data can be simulated, it is advantageous to make some simplifying assumptions. First, for GW detection, a signal-to-noise ratio threshold $\rho_*$ can be used as a proxy for signal selection threshold. For EM counterparts, there is no hope in pinpointing the counterpart and getting its host galaxy redshift without actively pointing a telescope at the relevant sky position. A number of complicated factors come into whether a telescope is pointed at the counterpart (e.g., a team's allotted observing time, weather conditions, camera field of view, etc.), but roughly speaking, GW events with small localization areas are more likely to be in an instrument's field of view than events with large localizations (e.g., Coughlin et al. 2019b, 2020).[2] The sky

[2] In some cases significant resources could be leveraged to cover large sky areas (e.g., Coughlin et al. 2019a), but this is unlikely to be the norm if observing resources remain constant and the detection rate of NS binaries increases due to increased interferometer sensitivity.

localization area of a GW signal approximately scales with $\rho^{-2}$ for moderately large $\rho$ (Fairhurst 2009), so we can model the selection function on the EM counterpart as depending on $\rho$ rather than the full $x_{\rm GW}$, which lets us replace instances of $x_{\rm GW}$ in Equation (9) with $\rho$ and integrate with respect to $\rho$ on interval $[\rho_*, \infty]$.

Now even if one or more telescopes are pointed at the true sky location of the event in question, it is not guaranteed that the EM counterpart will be detected, as the counterpart could be either misidentified or too dim (e.g., Kyutoku et al. 2020). This will depend sensitively on the observing strategies and detection pipelines that EM-follow-up groups employ, which again may be difficult to model. But for concreteness, let us consider a simple case: there is one EM-follow-up campaign that uses fixed exposure time and filters and a fixed detection pipeline that has detection threshold $\zeta_*$ on detection statistic $\zeta$, for which any observation with $\zeta \geqslant \zeta_*$ would be included in the analysis. The probability of EM detection assuming the instrument has been pointed at the source will not depend on the GW data or $\rho$, but it will depend on both the distance and redshift (hence a cosmology dependence) to the source because the source must at least be of significant brightness *in the relevant filters*. With these assumptions and a model of $\zeta$ given the source parameters, Equation (9) can be rewritten as

$$p_{\rm det}^{\rm EM,GW}(\boldsymbol{\theta}_{\rm EM}, \boldsymbol{\theta}, d_L, i, \tilde{z}) = \int_{\zeta_*}^{\infty} p(\zeta|\boldsymbol{\theta}_{\rm EM}, d_L, i, \tilde{z}, \in{\rm FOV}) \times \left[\int_{\rho_*}^{\infty} p(\in{\rm FOV}|\rho) p(\rho|\boldsymbol{\theta}, d_L, i, \tilde{z}) d\rho\right] d\zeta. \tag{10}$$

The first term in the outer integral of Equation (10) is the probability of getting EM detection statistic $\zeta$ given that the source was in the field of view of the EM instrument. This term depends on the specifics of the EM pipeline and the filters and exposure times chosen. The next term $p(\in{\rm FOV}|\rho)$ (in the integral in brackets) is the probability that the source was in the instrument field of view given the GW signal-to-noise ratio. This depends on how the EM instrument's field of view is pointed on the sky. In principle, Equation (10) is calculable, but careful modeling of each term is needed if the detection probability of sources changes across the prior range of the cosmological parameters.

## 3. Example

In this section, I perform a toy thunder-and-lightning $H_0$ inference using GW170817 and the AT2017gfo measured bolometric optical/near-infrared light curve from integration of the X-shooter spectra (Pian et al. 2017; Smartt et al. 2017). Given the cornucopia of modeling uncertainties in KN light curves and spectra, I opt to use a simple model for NS merger mass ejection and the associated KNe. The example herein, which is primarily for illustrative purposes, can be readily extended to multi-band light curve or spectral fits of KNe with more complex KN models, or even to other EM counterparts. I emphasize that other models, data, and assumptions could be made with respect to the following example, and that the choices made here were established to (a) demonstrate execution of the method and (b) demonstrate how reasonable changes to the underlying model significantly affect the inferences.

### 3.1. Data

Rather than performing full GW inference on the GW170817 strain, I re-weight the low-spin posterior samples from GW170817 provided by the Laser Interferometer Gravitational-Wave Observatory (LIGO)-Virgo Collaboration (LVC; LIGO Scientific Collaboration & Virgo Collaboration 2017).[3] For the bolometric light curves, I integrate the de-reddened, de-redshifted X-Shooter AT2017gfo optical/infrared spectra (Pian et al. 2017; Smartt et al. 2017).[4] Because the event is at such low redshift (even assuming a wide prior range on $H_0$), using the de-redshifted data here introduces negligible bias. In general though, such de-redshifted data cannot be used because it has already assumed a cosmology.

### 3.2. Model

Because I use the GW170817 posterior samples, the GW model and priors are already specified by the choices made in the LVC low-spin-prior analysis (LIGO Scientific Collaboration & Virgo Collaboration 2017), but other prior choices could be made if desired. To model the KN, I make the following assumptions, which are chosen mostly for simplicity of this example:

1. The KN ejecta velocity and opacity are fixed to $v = 0.25c$ and $\kappa = 1\ {\rm cm^2\ g^{-1}}$, respectively. The ejecta mass is calculated in two ways:
   (a) Using Equation (25) of Radice et al. (2018; which is modified to fit ejecta mass rather than disk mass):
   $$\frac{M_{\rm ej}}{M_\odot}(\tilde{\Lambda}) = \max\left\{10^{-4}, 0.0202 + 0.0341 \times \tanh\left(\frac{\tilde{\Lambda} - 538.8}{439.4}\right)\right\} \tag{11}$$
   $\tilde{\Lambda}$ is the binary tidal deformability parameter (e.g., LIGO Scientific Collaboration & Virgo Collaboration 2017)
   (b) Using Equations (1) and (2) of Dietrich & Ujevic (2017) to estimate a dynamical ejecta component and a disk wind ejecta prescription from Coughlin et al. (2019d) with a disk mass to ejecta mass conversion factor of 0.3.

Here, the parameters describing the KN $\boldsymbol{\theta}_{\rm EM}$ are fully specified by the binary parameters $\boldsymbol{\theta}$, so $p(\boldsymbol{\theta}_{\rm EM}|\boldsymbol{\theta}) = \delta(\kappa - 1\ {\rm cm^2\ g})\delta(v_{\rm ej} - 0.25c)\ \delta(M_{\rm ej} - M_{\rm ej}(\tilde{\Lambda}))$.

2. The KN bolometric luminosity is calculated for a single ejecta component using Equations (1) and (2) of Kashyap et al. (2019) and the prescriptions chosen therein. Furthermore, I assume that the KN bolometric luminosity has no viewing-angle dependence.[5]

### 3.3. Results

To calculate the posterior distribution on $H_0$, I re-weight the GW170817 posterior samples by (a) the KN light curve likelihood, which I take to be $\chi^2$ in the bolometric magnitudes with constant $\sigma = 1$ mag "modeling uncertainty" (similarly to Coughlin et al. 2019c), and (b) $p(v_r, \langle v_p\rangle|\tilde{z}, v_p)$ through prior

[3] https://dcc.ligo.org/LIGO-P1800061/public
[4] http://www.engrave-eso.org/AT2017gfo-Data-Release/
[5] Models with viewing-angle dependence could be used and indeed would help break distance-inclination degeneracy (Bulla 2019).

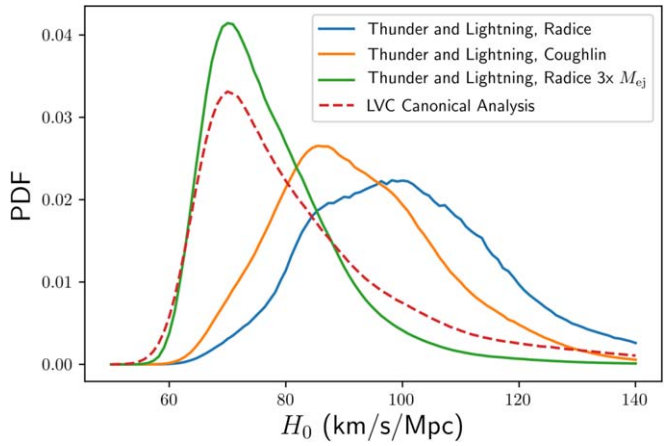


**Figure 1.** Posterior distributions on the Hubble constant $H_0$ for the LVC canonical analysis (Abbott et al. 2017b, but using the low-spin prior) and for thunder-and-lightning analyses. A thunder-and-lightning $H_0$ posterior is shown for the Radice et al. (2018) and Coughlin et al. (2019d) ejecta mass calculations, and for an ad hoc increase of their Radice et al. (2018) ejecta mass predictions of 3×.

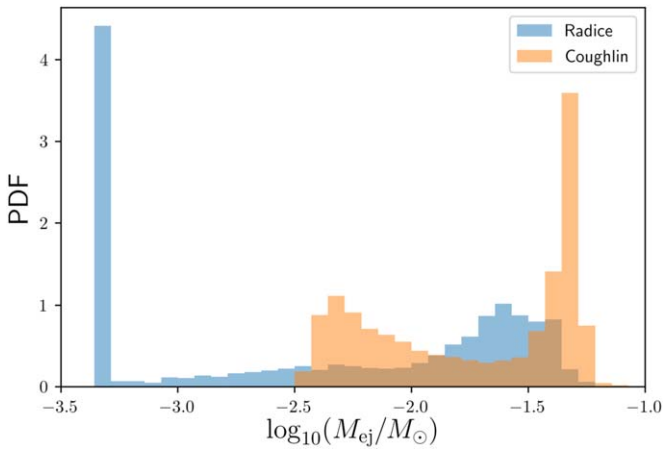


**Figure 2.** Ejecta masses calculated for the GW170817 posterior samples using prescriptions from Radice et al. (2018) and Dietrich & Ujevic (2017)/Coughlin et al. (2019d).

samples of $v_p$ and the prescriptions used in Abbott et al. (2017b). I use the same GW $H_0$ likelihood and velocity measurements as in Abbott et al. (2017b), as well as the same priors ($p(d_L) \sim d_L^2$, $p(H_0) \sim 1/H_0$, flat in component masses). The thunder-and-lightning reweighting of the GW170817 posterior samples yields the posterior distributions on $H_0$ shown in Figure 1. The blue and orange curves show the thunder-and-lightning $H_0$ inference using the Radice and Coughlin KN ejecta prescriptions, respectively. The green curve shows the results assuming three times the standard Radice ejecta mass. Note that these results incorporate the GW $H_0$ inference (shown in the dashed red line) via the original LVC GW samples and therefore should not be multiplied again by the LVC canonical analysis posterior.

## 4. Discussion

The comparison of $H_0$ posteriors shown in Figure 1 demonstrates the effects of different choices for the underlying EM model. With the toy model presented herein coupled with the Radice et al. (2018) ejecta mass prescription, the $H_0$ posterior favors higher expansion rates than the pure standard-siren method. This is due to the low ejecta masses predicted by Equation (11), shown in Figure 2, which favor a small source luminosity distance and hence a higher $H_0$. Using the ejecta masses from Dietrich & Ujevic (2017) and Coughlin et al. (2019d), yields similar results, albeit less biased to large $H_0$ since the predicted ejecta masses are larger. If the ejecta masses from Radice et al. (2018) are arbitrarily increased by a factor of 3, the inference on $H_0$ becomes consistent with those in the existing literature. It is also worth noting that these results would change if the high-spin analysis of the LVC were used instead. The take-away from this toy example is that the model of the KN and $p(\boldsymbol{\theta}_{\rm EM}|\boldsymbol{\theta})$ are crucially important to the thunder-and-lightning $H_0$ inference. I emphasize that the results shown here are not meant to be new constraints on the Hubble constant, but rather an illustration of the model dependence of thunder-and-lightning analyses.

### 4.1. Systematics, Populations, and Self-consistency

Coughlin et al. (2019c) performed the first thunder-and-lightning $H_0$ measurement with optical light curves and state-of-the-art models and find general agreement between their results and existing studies. However, as I have shown here, the underlying models used for the EM counterparts can greatly affect the Hubble constant measurement. As such, careful accounting of modeling uncertainties must be done to recover unbiased $H_0$ estimates. For KNe for example, ejecta properties can vary from study to study (Radice et al. 2018), so $H_0$ estimates may have large systematic errors. Also, selection effects must be addressed when the GW detector horizon distances extend to distances at which cosmology can affect the joint GW–EM detection prospects.

There are two other subtleties that must be addressed as well. First, if multiple joint GW–EM detections are brought to bear on $H_0$ in a combined thunder-and-lightning analysis, the compact-object-merger populations (e.g., distribution of NS masses) must be simultaneously fit with the cosmological parameters to account for degeneracy between the unknown population and the cosmology. This amounts to marginalizing over another set of variables $\boldsymbol{\lambda}$, which parameterize the NS mass and spin distributions. Without such a simultaneous fit, error in the assumed NS distributions will bias the inferred distances and hence the cosmology measurement.

Second, the models that go into thunder-and-lightning analyses should not be conditioned or trained on existing analyses or data sets that assume an underlying cosmology. For example, many analyses of AT2017gfo used a known cosmology to infer properties of the KN ejecta. If these inferred properties (e.g., KN ejecta velocity profile) are assumed in future thunder-and-lightning analyses, the results will not be self-consistent due to existing cosmological assumptions creeping in. Therefore, the simulations and models used for thunder-and-lightning analyses should rely only on general relativity, particle/nuclear theory, and fits to experiments that do not involve cosmology.

## 5. Conclusion

In this Letter, I have expanded on the work of Kashyap et al. (2019) and Coughlin et al. (2019c) by showing the full

Bayesian framework for thunder-and-lightning (joint GW–EM) inference of cosmological parameters. Additionally, I have described subtleties of such inferences that were not discussed in these previous works. In particular, thunder-and-lightning analyses must account for the following details.

1. Selection effects on the GW and EM data sets can potentially bias cosmological parameter measurements. These selection effects can be modeled under the right conditions.
2. Systematic errors in EM counterpart models can significantly bias cosmological measurements.
3. The degeneracy between the inferred underlying NS merger population and the cosmological parameters.
4. EM counterpart models that have been trained using a specific cosmology cannot be used as the cosmology itself is being inferred.

In all, the thunder-and-lightning method potentially has an exciting role to play in the ongoing cosmic controversy, but there are significant modeling challenges that must be overcome first.

I would like to thank the LVC for publicly releasing posterior samples and the ENGRAVE Collaboration for curating the X-Shooter AT2017gfo spectra. I acknowledge Michael Coughlin and Antonella Palmese for useful conversations and for reading a draft of this Letter.

*Software:* Matplotlib (Hunter 2007), Numpy (van der Walt et al. 2011), Scipy (Virtanen et al. 2019), gwemlightcurves (https://gwemlightcurves.github.io/).

## ORCID iDs

Zoheyr Doctor https://orcid.org/0000-0002-2077-4914

## References

Abbott, B. P., Abbott, R., Abbott, T. D., et al. 2017a, ApJ, 841, 89
Abbott, B. P., Abbott, R., Abbott, T. D., et al. 2017b, Natur, 551, 85
Abbott, B. P., Abbott, R., Abbott, T. D., et al. 2017c, ApJL, 850, L39
Abbott, B. P., Abbott, R., Abbott, T. D., et al. 2020, arXiv:2001.01761
Bulla, M. 2019, MNRAS, 489, 5037
Chen, H.-Y., Fishbach, M., & Holz, D. E. 2018, Natur, 562, 545
Coughlin, M. W., Ahumada, T., Anand, S., et al. 2019a, ApJL, 885, L19
Coughlin, M. W., Antier, S., Corre, D., et al. 2019b, MNRAS, 489, 5775
Coughlin, M. W., Dietrich, T., Antier, S., et al. 2020, MNRAS, 492, 863
Coughlin, M. W., Dietrich, T., Doctor, Z., et al. 2018, MNRAS, 480, 3871
Coughlin, M. W., Dietrich, T., Heinzel, J., et al. 2019c, arXiv:1908.00889
Coughlin, M. W., Dietrich, T., Margalit, B., & Metzger, B. D. 2019d, MNRAS, 489, L91
Del Pozzo, W. 2014, JPhCS, 484, 012030
Dhawan, S., Bulla, M., Goobar, A., Sagués Carracedo, A., & Setzer, C. N. 2020, ApJ, 888, 67
Dietrich, T., Khan, S., Dudi, R., et al. 2019, PhRvD, 99, 024029
Dietrich, T., & Ujevic, M. 2017, CQGra, 34, 105014
Doctor, Z., Kessler, R., Chen, H. Y., et al. 2017, ApJ, 837, 57
Fairhurst, S. 2009, NJPh, 11, 123006
Freedman, W. L. 2017, NatAs, 1, 0169
Guidorzi, C., Margutti, R., Brout, D., et al. 2017, ApJL, 851, L36
Harstad, E. D. 2013, PhD thesis, Oregon Univ., http://hdl.handle.net/1794/13003
Holz, D. E., & Hughes, S. A. 2005, ApJ, 629, 15
Hosseinzadeh, G., Cowperthwaite, P. S., Gomez, S., et al. 2019, ApJL, 880, L4
Hunter, J. D. 2007, CSE, 9, 90
Kasen, D., Metzger, B., Barnes, J., Quataert, E., & Ramirez-Ruiz, E. 2017, Natur, 551, 80
Kashyap, R., Raman, G., & Ajith, P. 2019, ApJL, 886, L19
Kyutoku, K., Fujibayashi, S., Hayashi, K., et al. 2020, ApJL, 890, L4
Lackey, B. D., Pürrer, M., Taracchini, A., & Marsat, S. 2019, PhRvD, 100, 024002
LIGO Scientific Collaboration & Virgo Collaboration 2017, PhRvL, 119, 161101
Metzger, B. D. 2019, LRR, 23, 1
Mortlock, D. J., Feeney, S. M., Peiris, H. V., Williamson, A. R., & Nissanke, S. M. 2019, PhRvD, 100, 103523
Pian, E., D'Avanzo, P., Benetti, S., et al. 2017, Natur, 551, 67
Planck Collaboration 2018, arXiv:1807.06209
Radice, D., Perego, A., Hotokezaka, K., et al. 2018, ApJ, 869, 130
Riess, A. G., Macri, L. M., Hoffmann, S. L., et al. 2016, ApJ, 826, 56
Schutz, B. F. 1986, Natur, 323, 310
Scolnic, D., Kessler, R., Brout, D., et al. 2018, ApJL, 852, L3
Smartt, S. J., Chen, T. W., Jerkstrand, A., et al. 2017, Natur, 551, 75
Soares-Santos, M., Palmese, A., Hartley, W., et al. 2019, ApJL, 876, L7
van der Walt, S., Colbert, S. C., & Varoquaux, G. 2011, CSE, 13, 22
Virtanen, P., Gommers, R., Oliphant, T. E., et al. 2019, arXiv:1907.10121